Published in final edited form as:

Hepatology. 2022 April ; 75(4): 797–813. doi:10.1002/hep.32233.

MT1 but not MT2 melatonin receptor knockout decreases biliary damage and liver fibrosis during cholestatic liver injury

Nan Wu[1], **Guido Carpino**[2], **Ludovica Ceci**[1], **Leonardo Baiocchi**[3], **Heather Francis**[1,4], **Lindsey Kennedy**[1,4], **Tianhao Zhou**[1], **Lixian Chen**[1], **Keisaku Sato**[1], **Konstantina Kyritsi**[1], **Vik Meadows**[1], **Burcin Ekser**[5], **Antonio Franchitto**[6], **Romina Mancinelli**[6], **Paolo Onori**[6], **Eugenio Gaudio**[6], **Shannon Glaser**[7,#], **Gianfranco Alpini**[1,4,#]

[1]Hepatology and Gastroenterology, Medicine, Indiana University, Indianapolis, IN,

[2]Department of Movement, Human and Health Sciences, Division of Health Sciences, University of Rome “Foro Italico”, Rome, Italy,

[3]Hepatology Unit, University of Tor Vergata, Rome, Italy,

[4]Richard L. Roudebush VA Medical Center, Indianapolis, IN,

[5]Division of Transplant Surgery, Department of Surgery, Indiana University, Indianapolis, IN,

[6]Department of Anatomical, Histological, Forensic Medicine and Orthopedics Sciences, Sapienza University of Rome, Rome, Italy,

[7]Department of Medical Physiology, Texas A&M University College of Medicine, Bryan, TX,

Abstract

Background & aims: Melatonin reduces biliary damage and liver fibrosis in cholestatic models by interaction with melatonin receptors, MT1 and MT2. MT1 and MT2 can form hetero- and homo-dimers, but MT1 and MT2 can heterodimerize with the orphan receptor, G protein-coupled receptor 50 (GPR50). MT1/GPR50 dimerization blocks melatonin binding, but MT2/GPR50 dimerization does not affect melatonin binding. GPR50 can dimerize with transforming growth factorβ receptor type I (TGFβRI) to activate this receptor. We aimed to determine the differential roles of MT1 and MT2 during cholestasis.

Approach & Results: Wild-type (WT), MT1 knockout (KO), MT2KO and MT1/MT2 double KO (DKO) mice underwent sham or bile duct ligation (BDL); these mice were also treated with melatonin. BDL WT and Mdr2$^{-/-}$ mice received mismatch, MT1 or MT2 Vivo-Morpholino. Biliary expression of MT1 and GPR50 increases in cholestatic rodents and human primary sclerosing cholangitis (PSC) samples. Loss of MT1 in BDL and Mdr2$^{-/-}$ mice ameliorated biliary and liver damage, whereas these parameters were enhanced following loss of MT2 and in DKO mice. Interestingly, melatonin treatment alleviated BDL-induced biliary and liver injury in BDL WT and BDL MT2KO mice, but not BDL MT1KO or BDL DKO mice, demonstrating melatonin

Address correspondence to: Gianfranco Alpini, Ph.D., Professor of Medicine, VA Senior Research Scientist, Hickam Endowed Chair, Director, Indiana Center for Liver Research, Richard L. Roudebush VA Medical Center and Indiana University, Gastroenterology, Medicine, 702 Rotary Circle, Indianapolis, IN 46202, galpini@iu.edu.
[#]Drs. Glaser and Alpini share the senior authorship

interaction with MT1. Loss of MT2 or DKO mice exhibited enhanced GPR50/TGFβR1 signaling, which was reduced by loss of MT1.

Conclusions: Melatonin ameliorates liver phenotypes via MT1, whereas downregulation of MT2 promotes liver damage via GPR50/TGFβR1 activation. Blocking GPR50/TGFβR1 binding via modulation of melatonin signaling may be a therapeutic approach for PSC.

Keywords

cellular senescence; protein kinase A; primary sclerosing cholangitis; TGFβ1

Introduction

Cholangiocytes are the target cells in several cholangiopathies such as primary sclerosing cholangitis (PSC) and primary biliary cholangitis (PBC), diseases that are evidenced by changes in intrahepatic biliary mass (IBDM), biliary senescence and liver fibrosis, phenotypes that are regulated by several factors including melatonin (1, 2).

Melatonin is secreted from the pineal gland and peripheral organs such as the gastrointestinal and biliary tract (1, 3). Three different melatonin receptors have been identified, with melatonin receptors 1A and 1B (MT1 and MT2) that are expressed in mammalian tissue and melatonin receptor 1C in amphibians (4). G Protein-Coupled Receptor 50 (GPR50) is a melatonin-related orphan receptor with no affinity for melatonin (5). GPR50 can heterodimerize constitutively with MT1, MT2 and transforming growth factor-β (TGFβ) receptor type I (TGFβR1); GPR50 dimerization with MT1 (MT1/GPR50) inhibits melatonin binding to MT1, but GPR50 dimerization with MT2 (MT2/GPR50) does not block MT2 melatonin signaling (6). Engagement of GPR50 into heterodimers with TGFβR1 activates this receptor independent of TGFβ binding (7).

In addition to regulating central circadian activity, melatonin modulates the function of several peripheral organs including the biliary epithelium by interacting with MT1 and MT2 (8); however, the differential role of MT1 and MT2 in cholestatic liver injury is unknown. We have previously shown that: (i) the rate limiting-step enzymes for melatonin synthesis (arylalkylamine N-acetyltransferase, AANAT, and acetylserotonin O-methyltransferase) modulate biliary phenotypes during cholestasis by autocrine signaling (1, 8, 9); and (ii) exposure to complete darkness (which increases melatonin secretion) or exogenous melatonin administration ameliorates the phenotypes of the multidrug resistance 2 knockout ($Mdr2^{-/-}$) mouse model of PSC (8, 10). We aimed to determine: (i) the differential effects of MT1 and MT2 on biliary/liver phenotypes; and (ii) the effect of melatonin treatment on biliary damage and liver fibrosis in MT1 and MT2 KO mice.

Materials and Methods

Materials

Reagents were purchased from Sigma-Aldrich Chemical Co. (St. Louis, MO) unless otherwise indicated. Information for all antibodies used is described in Supplemental Table 1. RNAs were extracted using TRIZOL® Reagent (Ambion®-Life Technologies, Grand

Island, NY) following the manufacturer's instructions. The Nova Ultra Sirius Red Stain kit to detect interstitial collagen deposition was purchased from IHC World (Woodstock, MD). The information on real-time PCR primers used is listed in Supplemental Table 2.

Animal Models

Male MT1KO and MT2KO mice (~25–30 g, obtained from Dr. G. Tosini, Morehouse School of Medicine, Atlanta, GA) were crossed until homozygous MT1 and MT2 DKO mice were obtained; the breeding colonies for MT1KO, MT2KO and DKO mice are established in our animal facility. The corresponding wild-type mice (WT, C3H/HeJ) were obtained from Dr. G. Tosini. In the first set of experiments, WT, MT1KO, MT2KO and DKO mice (12 wk of age) underwent sham surgery or bile duct ligation (BDL) for 1 wk (11). To support the findings from MT1KO, MT2KO and DKO mice, we treated: (i) BDL WT mice with Vivo-Morpholino sequences of MT1 (5'-GCAGCTCGCTGACATTGCCCTTCAT, to reduce MT1 expression) and/or MT2 (5'-GGATTGAGCTGTTCTCAGGCATCTC, to reduce MT2 expression) or mismatch Morpholino (5'-GaAGCTaGCTcACATTGaCCTTaAT, for MT1, and 5'- GcATTcAGCTGTTaTCAGcCATaTC, for MT2) (Gene Tools LCC, Philomath, OR) via tail vein injections (12.5 mg/kg body weight) at 1 and 4 days post sham or BDL surgery; and (ii) $Mdr2^{-/-}$ mice (FVB/NJ inbred mice, 12 wk of age) with MT1 (5'-GCAGCTCGCTGACATTGCCCTTCAT, to reduce the expression of MT1) or mismatch Morpholino (5'-GaAGCTaGCTcACATTGaCCTTaAT) via tail vein injections (at 7 and 3 days prior to harvesting, at the dose of 12.5 mg/kg body weight). Following the administration of the mismatch Morpholino or Vivo-Morpholino targeting MT1, MT2 or MT1/MT2, we evaluated the immunoreactivity of MT1 and MT2 by semiquantitative immunohistochemistry in paraffin-embedded liver sections (4 μm thick). Since MT1 immunoreactivity is present in cholangiocytes and at lower level in hepatic stellate cells (HSCs), but not hepatocytes (3) and since MT1 is upregulated in cholangiocytes from BDL and $Mdr2^{-/-}$ mice (see Figure 1), the administration of MT1 Vivo-Morpholino likely selectively targets cholangiocytes. To determine if melatonin's effects are mediated by a selective interaction with MT1 or MT2, we treated WT, MT1KO, MT2KO, and DKO mice subjected to sham or BDL surgery with melatonin (dissolved in drinking water, 20 mg/L corresponding to a melatonin intake of 3 μg/g body weight per day) (12) for 1 wk. Animals were maintained in a temperature-controlled environment (20–22°C) with 12:12-hour light/dark cycles with free access to food and drinking water. Animal experiments were performed according to protocols approved by either the Baylor Scott & White Health or Indiana University School of Medicine IACUC Committees.

Human PSC samples

Human liver samples were obtained from the following sources: (i) controls (n=3, "n" is used to designate sample size from each population) were purchased from Sekisui Xeno Tech (Kansas City, KS); (ii) another control (n=1) and PSC samples (stage 4, late-stage, n=6) were obtained from Dr. Burcin Ekser under the Institutional Review Board approved protocol at Indiana University School of Medicine. The samples were used for RNA extraction, paraffin-embedded and frozen sections. Informed consent was collected from patients for the human specimens that were utilized in this study. The characteristics of human control and PSC samples are listed in Supplemental Table 3.

Cholangiocytes and HSCs

Mouse cholangiocytes were isolated by immunoaffinity separation (1, 2) using a monoclonal antibody, rat IgG2a (from Dr. R. Faris, Providence, RI) against an antigen expressed by all intrahepatic cholangiocytes. HSCs were isolated by laser capture microscopy (LCM) (13) from frozen liver sections (10 μm thick) from 3 different mice for each group (n=3), incubated overnight with an antibody against desmin (HSC marker) (14); desmin-positive cells were dissected from the slides by the LCM system Leica LMD7000 (Buffalo Grove, IL) and collected into PCR tubes. Cholangiocytes from human samples were isolated by LCM with cytokeratin-19 (CK-19) antibody (biliary marker) (11). Total RNA was extracted with the Arcturus PicoPure RNA isolation kit (Thermo Fisher Scientific, Waltham, MA).

Statistical analysis

All data are expressed as mean ± standard error (SEM). Differences between groups were analyzed by unpaired Student's *t* test during analysis of two groups and one-way ANOVA when more than two groups were analyzed, followed by a suitable *post hoc* test. The level of significance was set at $P<0.05$.

Detailed descriptions for all other experimental procedures are described in the Supplemental Information.

Results

Immunoreactivity/expression of MT1 and MT2

By immunofluorescence in liver sections, we demonstrated biliary immunoreactivity for MT1 and MT2 in WT and BDL WT (C3H/HeJ) mice, $Mdr2^{-/-}$ mice and its corresponding WT (FVB/NJ WT) mice, and in human samples from control subjects and PSC patients (Figure 1A–C). We demonstrated weak immunoreactivity for MT1 and MT2 in mouse and human HSCs (co-stained for desmin), whereas mouse hepatocytes (co-stained for hepatocyte nuclear factor 4α, HNF4α) were negative for MT1 and MT2 (Figure 1A–C).

By immunohistochemistry in liver sections, we demonstrated immunoreactivity of MT1 and MT2 in bile ducts from WT and BDL WT mice (Supplemental Figure 1A). Concomitant with loss of MT1 in MT1KO mice, there was enhanced immunoreactivity of MT2 in cholangiocytes, whereas in MT2KO mice there was enhanced biliary MT1 immunoreactivity (Supplemental Figure 1A). A similar profile in mRNA expression of MT1 and MT2 was seen in cholangiocytes from the selected groups of mice (Supplemental Figure 1B). We observed enhanced mRNA expression of MT1 ($P<0.05$) but not MT2 ($P=0.64$) in cholangiocytes from PSC patients compared to controls (Supplemental Figure 1C). These findings demonstrate a compensatory regulation of MT1 and MT2 following the loss of the receptor subtypes during cholestatic liver injury.

Measurement of immunoreactivity/mRNA expression of AANAT and melatonin serum levels

In agreement with previous studies (1, 3), we observed immunoreactivity for AANAT in bile ducts from BDL WT and $Mdr2^{-/-}$ mice as well as late-stage PSC patients

(likely due a compensatory mechanism), compared to the corresponding control samples (Supplemental Figure 2A–B). Parallel to our previous study (3), we did not detect AANAT immunoreactivity (co-localized with desmin) in HSCs (Supplemental Figure 2A).

There was enhanced biliary AANAT mRNA expression and melatonin serum levels in BDL WT compared to WT mice; these parameters were unchanged in BDL MT1KO compared to BDL WT mice, but decreased in BDL MT2KO compared to BDL WT mice (Supplemental Figure 2C); BDL DKO mice displayed reduced biliary AANAT mRNA expression compared to BDL WT mice (Supplemental Figure 2C).

BDL-induced liver damage is ameliorated in MT1KO but aggravated in MT2KO mice

Histopathological examination by hematoxylin and eosin (H&E) staining revealed foci of hepatocyte necrosis (score=2) and moderate portal inflammation (score=2) in BDL WT mice (Supplemental Figure 3A); however, BDL MT1KO mice showed a lower number of foci of necrosis (score=1) and mild inflammation (score=1) than BDL WT mice. Interestingly, both MT2KO and MT1/MT2 DKO BDL mice showed a higher degree of hepatocyte necrosis (score=3) and marked inflammation (score=3) compared to BDL WT mice; WT mice had normal histology (Supplemental Figure 3A). There were no relevant changes in the histology of stomach, small and large intestine, pancreas, lung, heart, spleen, and kidney among WT, MT1KO, MT2KO and DKO mice after sham or BDL surgery (Supplemental Figure 3C).

IBDM and liver fibrosis are decreased in MT1KO but increased in MT2KO and DKO mice following BDL

IBDM was similar between WT, MT1KO, and MT2KO mice (Figure 2A). There was increased IBDM in BDL WT compared to WT mice, which was reduced in BDL MT1KO mice, but increased in BDL MT2KO and BDL DKO mice (Figure 2A). We demonstrated: (i) enhanced collagen deposition and immunoreactivity for α-smooth muscle actin (α-SMA) and collagen type I (Col1) in BDL WT compared to WT mice; (ii) reduced liver collagen deposition and immunoreactivity for α-SMA and Col1 in BDL MT1KO compared to BDL WT mice; but (iii) increased collagen deposition and immunoreactivity for α-SMA and Col1 in BDL MT2KO and BDL DKO compared to BDL WT mice (Figure 2B–C); no significant changes in collagen deposition were observed in the sham-operated groups (Figure 2B). The mRNA expression of α-SMA, collagen type I, alpha 1 (Col1a1) and fibronectin-1 (Fn-1), increased in cholangiocytes and HSCs from BDL WT compared to WT mice (Figure 2D); however, mRNA expression of these markers decreased in MT1KO but were enhanced in MT2KO mice following BDL (Figure 2D).

Differential effects of MT1 and MT2 on cholangiocyte and HSC senescence and liver inflammation

Biliary senescence activates HSCs by paracrine mechanisms through release of senescence-associated secretory phenotypes (SASPs, e.g., TGFβ1), whereas activation of cellular senescence in HSCs limits liver fibrosis (15). Senescence-associated β-galactosidase (SA-β-gal) staining and immunofluorescence for cyclin-dependent kinase inhibitor 2A (p16, co-stained with CK-19) demonstrated increased biliary senescence in BDL WT compared to WT mice, which was reduced in BDL MT1KO but increased in BDL MT2KO mice

compared to BDL WT mice (Figure 3A–B); biliary senescence was further increased in BDL DKO compared to BDL WT mice (Figure 3B). By real-time PCR for p16 and cyclin-dependent kinase inhibitor 1A (p21), we demonstrated: (i) increased biliary but reduced HSC senescence in BDL WT mice and BDL MT2KO compared to WT and BDL WT mice, respectively; and (ii) reduced biliary senescence and increased HSC senescence in BDL MT1KO compared to BDL WT mice (Figure 3C). There was increased number of F4/80-positive macrophages in BDL WT compared to WT mice, which decreased in BDL MT1KO but increased in BDL MT2KO and BDL DKO mice compared to BDL WT mice (Supplemental Figure 4A).

Evaluation of miR-200b-dependent angiogenesis and clock genes

There was increased immunoreactivity for platelet endothelial cell adhesion molecule (CD31) in BDL WT compared to WT mice, which decreased in BDL MT1KO but increased in BDL MT2KO and BDL DKO mice compared to BDL WT mice (Supplemental Figure 5A). The expression of miR-200b increased in cholangiocytes from BDL WT compared to WT mice, which decreased in BDL MT1KO mice (Supplemental Figure 5C).

We demonstrated: (i) increased immunoreactivity of brain and muscle ARNT-Like 1 (Bmal1) in liver sections and mRNA expression of circadian locomotor output cycles kaput (Clock), Bmal1, cryptochrome 1 (Cry1) and period circadian clock 1 (Per1) in cholangiocytes from BDL WT compared to WT mice that were reduced in BDL MT1KO but enhanced in BDL MT2KO and BDL DKO mice (Supplemental Figure 6A and C).

Effects of MT1 and/or MT2 Vivo-Morpholino on liver phenotypes of BDL and Mdr2$^{-/-}$ mice

In liver sections, we demonstrated: (i) decreased immunoreactivity of MT1 and MT2 in BDL WT mice treated with MT1, MT2 or MT1/MT2 Vivo-Morpholino, respectively, compared to the corresponding mismatch Morpholino (Figure 4A); and (ii) decreased immunoreactivity of MT1 in Mdr2$^{-/-}$ mice treated with MT1 Vivo-Morpholino compared to Mdr2$^{-/-}$ mice treated with MT1 mismatch Morpholino (Figure 5A). We demonstrated increased serum levels of alkaline phosphatase (ALP) in Mdr2$^{-/-}$ compared to WT mice, which was decreased in Mdr2$^{-/-}$ mice treated with MT1 Vivo-Morpholino compared to Mdr2$^{-/-}$ mice treated with MT1 mismatch Morpholino; no significant changes in the levels of transaminases (markers of hepatocyte injury, except the increase in alanine aminotransferase (ALT) in Mdr2$^{-/-}$ mice) were observed in the other animal groups (Supplemental Table 5). There was: (i) reduced liver damage (Supplemental Figure 3B), IBDM, liver fibrosis, biliary senescence (Figure 4B–D), inflammation, angiogenesis, immunoreactivity of Bmal1, and biliary expression of clock genes and miR-200b, in BDL WT mice treated with MT1 Vivo-Morpholino compared to BDL WT mice treated with MT1/MT2 mismatch Morpholino (Supplemental Figure 4B, 5B–C and 6B–C); (ii) increased liver damage (Supplemental Figure 3B), IBDM, liver fibrosis, biliary senescence (Figure 4B–D), inflammation, angiogenesis, immunoreactivity of Bmal1 and biliary expression of clock genes, inflammation and angiogenesis in BDL WT mice treated with MT2 and MT1/MT2 Vivo-Morpholino compared to BDL WT mice treated with MT1/MT2 mismatch Morpholino (Supplemental Figure 4B, 5B and 6B–C); and (iii) reduced liver damage, IBDM, biliary senescence, liver fibrosis (Figure 5A–C), inflammation, angiogenesis,

immunoreactivity of Bmal1 and biliary expression of clock genes and miR-200b in Mdr2$^{-/-}$ mice treated with MT1 Vivo-Morpholino compared to Mdr2$^{-/-}$ mice treated with mismatch Morpholino (Supplemental Figure 4B, 5B–C and 6B–C).

Effect of melatonin on liver phenotypes in BDL WT, MT1KO, MT2KO and DKO mice

Our previous *in vitro* studies showed that melatonin inhibits biliary hyperplasia by interaction with MT1 (2). In addition to the interaction with MT1, melatonin interacts with the nuclear receptor superfamily RZR/ROR (16) demonstrating a receptor-independent signaling mechanism. Supporting our *in vitro* studies (2), we demonstrated that melatonin significantly reduces liver damage (Supplemental Figure 3A), IBDM (Figure 6A), biliary senescence (Figure 6B), liver fibrosis (Figure 6C), liver inflammation, angiogenesis and immunoreactivity of Bmal1 in BDL WT and BDL MT2KO mice, but not in BDL MT1KO and BDL DKO mice (Supplemental Figure 3A, 4A, 5A, 6A). Our data support the concept that a selective interaction with MT1 mediates the beneficial effects of melatonin on liver phenotypes.

Evaluation of protein kinase A (PKA) phosphorylation in liver sections and cholangiocytes

We demonstrated increased biliary expression of p-PKA substrate in liver sections (co-stained with CK-19) from BDL WT compared to WT mice, which was decreased in BDL MT1KO mice but further enhanced in both BDL MT2KO and BDL DKO mice compared to BDL WT mice (Supplemental Figure 7A and Supplemental Table 4). Administration of melatonin decreased the biliary immunoreactivity of p-PKA in liver sections from BDL WT and BDL MT2KO mice, but not of BDL MT1KO and BDL DKO mice (Supplemental Figure 7A and Supplemental Table 4). Mdr2$^{-/-}$ mice displayed biliary p-PKA immunoreactivity compared to control mice, which were reduced in Mdr2$^{-/-}$ mice treated with MT1 Vivo-Morpholino compared to Mdr2$^{-/-}$ mice treated with MT1 mismatch Morpholino (Supplemental Figure 7B and Supplemental Table 4).

We demonstrated enhanced biliary p-PKA immunoreactivity in PSC samples compared to controls (Supplemental Figure 7C and Supplemental Table 4). A profile similar to that observed for p-PKA substrate immunoreactivity was observed by immunoblots for p-PKA/PKA (expressed as ratio to GAPDH) in cholangiocytes from WT, MT1KO and MT2KO mice after sham or BDL surgery (Supplemental Figure 7D). However, there was no significant change in ratios of p-PKA/PKA among WT, MT1KO and MT2KO mice after sham or BDL surgery (Supplemental Figure 7D), suggesting that knockout of MT1 or MT2 regulates PKA protein levels rather than directly controlling the rates of PKA phosphorylation.

Measurement of GPR50 immunoreactivity/expression and TGFβR1 activation

GPR50 acts as a melatonin-related orphan receptor but has no affinity to melatonin (5), and GPR50 heterodimerization with MT1 inhibits melatonin binding to MT1 (6). In addition, engagement of GPR50 into heterodimers with TGFβR1 activates this receptor independent of TGFβ binding (7). To demonstrate that the changes in liver phenotypes, due to the loss of MT1 or MT2, are GPR50/TGFβR1-dependent, we evaluated the immunoreactivity/expression of GPR50, TGFβR1 and phosphorylation of Smad3 (p-Smad3). We demonstrated

immunoreactivity for GPR50 in cholangiocytes, TGFβR1 and p-Smad3 in cholangiocytes and total liver from all mouse groups, which was enhanced in (i) BDL WT compared to WT mice, (ii) BDL MT2KO and BDL DKO compared to BDL WT mice, (iii) BDL WT mice treated with MT2 and MT1/MT2 Vivo-Morpholino compared to BDL WT mice treated with MT1/MT2 mismatch Morpholino (Figure 7A); (iv) $Mdr2^{-/-}$ compared to control mice; and (v) PSC samples compared to controls (Figure 7B). Biliary GPR50, TGFβR1 and p-Smad3 immunoreactivity was reduced in (i) BDL MT1KO mice compared to BDL WT mice, (ii) BDL WT mice treated with MT1 Vivo-Morpholino compared to BDL WT mice treated with MT1/MT2 mismatch Morpholino (Figure 7A) and (iii) $Mdr2^{-/-}$ mice treated with MT1 Vivo-Morpholino compared to $Mdr2^{-/-}$ mice treated with MT1 mismatch Morpholino (Figure 7B). TGFβ1 levels increased in cholangiocyte supernatants from BDL WT and $Mdr2^{-/-}$ mice compared to WT mice but decreased in BDL MT1KO mice compared to BDL WT mice and $Mdr2^{-/-}$ mice treated with MT1 mismatch Morpholino (Figure 7C). Similar trends were demonstrated by real-time PCR for GPR50 mRNA expression in isolated mouse cholangiocytes and in human PSC liver, and for TGFβR1 and TGFβ1 in mouse cholangiocytes (Figure 7D). No significant changes in GPR50 were observed after melatonin treatment in the BDL animal groups (Figure 7A, D), supporting the concept that downregulation of melatonin/MT1 signaling ameliorates biliary damage and liver phenotypes.

Measurement of bile acid levels and composition in liver tissue

Knockout of MT1 caused the liver content of taurocholic acid (TCA) in the total bile acid pool to significantly drop from 54.91% to 39.45% and content of tauro-β-muricholic acid (T-β-MCA) within the total bile acid pool to rise from 42.01% to 57.37% following BDL (Supplemental Figure8); a similar trend was also found in $Mdr2^{-/-}$ mice treated with MT1 Vivo-Morpholino compared to $Mdr2^{-/-}$ mice treated with MT1 mismatch Morpholino (Supplemental Figure 8). In the livers of WT and BDL MT1KO mice there was a decrease in the levels of glyco lithocholic acid (GLCA) compared to WT and BDL WT mice; the levels of deoxycholic acid (DCA) were decreased in BDL MT1KO compared with BDL WT mice (Supplemental Table 6). There were no significant changes in liver total bile acid levels and total primary/secondary conjugated/unconjugated bile acid levels between all BDL mouse groups (Supplemental Table 7). Treatment of $Mdr2^{-/-}$ mice with MT1 Vivo-Morpholino significantly changed bile acid levels of taurochenodeoxycholic acid (TCDCA), TβMCA, tauroursodeoxycholic acid (TUDCA) and tauro-ω-muricholic acid (T-ω-MCA) as well as total secondary bile acids and total secondary conjugated bile acids (Supplemental Tables 8 and 9).

Discussion

This study relates to the differential effect of the melatonin/MT1/MT2 axis on PKA signaling and activation of TGFβ/TGFβR1 signaling via GPR50 binding in the modulation of PSC phenotypes. We demonstrated that: (i) knockout of MT1 ameliorates the phenotypes of cholestatic injury, whereas knockout of MT2 or both MT1and MT2 (DKO) worsens biliary injury and liver fibrosis; and (ii) the administration of melatonin rescues liver phenotypes in MT2KO but not MT1KO and DKO BDL mice, demonstrating that the

beneficial effects of melatonin on PSC phenotypes are primarily mediated by interaction with MT1.

Supporting our findings, recent work has shown that melatonin inhibits biliary hyperplasia in BDL rats by downregulation of MT1 through decreased PKA phosphorylation (2). This finding was mainly derived by *in vitro* experiments using Luzindole and 4P-PDOT, the first being an unselective MT1/MT2 antagonist and the second showing a higher affinity (around 1000-fold) for MT2. To identify the differential role of MT1 and MT2 during cholestasis, we performed experiments in BDL and Mdr2$^{-/-}$ mice following genetic knockout or pharmacological inhibition of MT1, MT2 or both receptors. In a recent study, MT2 but not MT1 was involved in mitigating myocardial ischemia/reperfusion injury, and the cardio-protection mediated by MT2 was independent of the presence of melatonin (17). Another study suggests that melatonin enhanced cell-mediated and humoral immune functions through MT2, but not MT1 (18). Conversely, as observed for other G-protein coupled receptors, MT1 and MT2 may undergo differential desensitization or internalization according to their natural agonist's concentration or time of exposure, leading to a reduced biological response (19, 20). Thus, the possibility to explore the differential effects of MT1 and MT2 on liver phenotypes seemed a natural progression of our previous studies.

In addition to being expressed in the central nervous system, studies demonstrated the presence of MT1 and MT2 in peripheral organs such as pancreas and the biliary epithelium (2, 21). The increased immunoreactivity/expression of MT1 (observed in cholestatic BDL and Mdr2$^{-/-}$ mice and human PSC samples) supports the concept that MT1 is a key pharmacological target for ameliorating cholestatic liver injury. The discrepancy between the increase in MT2 expression (observed in our previous study in human PSC lines) (3) and our finding related to MT2 expression in human PSC samples may be due to the different models used (*in vitro* and *in vivo*) and the fact that total liver samples from human PSC specimen contain other cell types compared to the immortalized pure human PSC cell line. Furthermore, some studies support the absence/weak expression of melatonin receptors in hepatocytes, whereas others show the presence of MT1 in pericentral but not periportal hepatocytes (2, 22). Concerning the expression of melatonin receptors in HSCs, we demonstrated weak immunoreactivity of MT1 in HSCs from cholestatic BDL rats, and MT1 and MT2 in HSCs from BDL and Mdr2$^{-/-}$ mice (current study) as well as HSC lines (3). Conversely, quiescent and activated HSCs express the nuclear melatonin sensor retinoic acid receptor-related orphan receptor-alpha (RORα/Nr1f1) but not MT1 and MT2 (23).

The fact that AANAT is mainly expressed in cholangiocytes provides support the concept that AANAT/melatonin/MT1/MT2/PKA signaling modulates biliary damage (by an autocrine pathway), liver inflammation and fibrosis by paracrine mechanisms through changes in the biliary release of SASPs (15, 24, 25). Our results are supported by a recent study demonstrating increased immunoreactivity/expression of AANAT in cholangiocytes (likely due to a compensatory mechanism) from cirrhotic PBC specimen, whereas melatonin biosynthesis and levels were reduced (26). The concept related to melatonin's autocrine modulation of liver phenotypes is supported by previous studies showing that the biliary modulation of AANAT regulates liver phenotypes in cholestatic rodent models and human cholangiocarcinoma *in vitro* and *in vivo* models (1, 3, 9). The presence of AANAT has

been demonstrated in other peripheral organs such as spleen, kidney and heart (27). Melatonin ameliorates biliary damage and senescence as well as liver inflammation, fibrosis and cirrhosis through receptor-dependent and -independent pathways (1–3, 8). For example, melatonin ameliorates the phenotypes of liver diseases such as early-stage and late-stage liver cirrhosis, non-alcoholic fatty liver diseases (NAFLD), nonalcoholic steatohepatitis (NASH), alcohol-induced liver damage, PBC and PSC through antioxidant and anti-inflammatory properties (8, 10, 28, 29).

MT1 and MT2 homodimers are tightly coupled to the G_i/cAMP/p-PKA pathway, which appears to be the case for MT1/MT2 heterodimers (30), a concept supported by our data showing melatonin ameliorates liver phenotypes through downregulation of MT1/cAMP/p-PKA signaling. For example, the melatonin/MT1 axis modulates insulin secretion in rat pancreatic cells through downregulation of cAMP levels (31). Upregulation of hepatic melatonin levels by overexpression of the biliary AANAT inhibited biliary damage in cholestatic rodents by downregulation of cAMP signaling (1). Furthermore, melatonin decreases the proliferation of the hepatocarcinoma HepG2 cell line by downregulation of the cAMP/p-PKA signaling pathway (32). Supporting the notion that downregulation of MT1 decreases cAMP signaling, a study has shown that the pharmacological effects of melatonin on HEK-293 cells are mediated by MT1-dependent activation of ERK1/2 (33). The concept that the lack of or downregulation of MT2 would result in increased cAMP signaling and subsequent worsened liver phenotypes is supported by evidence in chick embryo retinas where melatonin inhibition of cAMP levels was blocked by the MT2 antagonist, 4-phenyl-2-propionamidotetralin (34). Furthermore, we aimed to determine if knockout of MT1 or MT2 affected the expression of GPR50/TGFβ1R signaling and subsequent changes in biliary and liver phenotypes. GPR50 is a melatonin-related orphan receptor with no affinity to melatonin (5), and GPR50 can heterodimerize with MT1, MT2 and TGFβRI. However, GPR50 dimerization with MT1 (MT1/GPR50) completely inhibits melatonin binding of MT1, but GPR50 dimerization with MT2 (MT2/GPR50) does not reduce melatonin binding to MT2 (6). Engagement of GPR50 into heterodimers with TGFβR1 (GPR50/TGFβR1) activates TGFβ signaling independent of TGFβ levels (7). Our data showed that the expression of GPR50 was increased in cholangiocytes from $Mdr2^{-/-}$ mice and PSC human samples which may promote the activation of TGFβ signaling. Interestingly, the propensity for MT1/MT1 homodimer and MT1/MT2 heterodimer formation is similar and predominant, whereas the propensity for MT2/MT2 homodimer formation is much lower (35). Therefore, depletion of MT1 may lead to increased MT2/GPR50 heterodimer formation and subsequently reduce GPR50/TGFβR1 heterodimer-induced TGFβ signal activation. In fact, following the knockout of MT2, there is enhanced likelihood of MT1/MT1 homodimer and MT1/GPR50 heterodimer formation that completely inhibits melatonin binding of MT1 (6), which explains why MT2KO mice subjected to cholestatic injury have worse biliary and liver phenotypes. In support of this concept, knockout of MT1 decreases GPR50, whereas MT2 knockout increases GPR50 expression. The differential changes in biliary expression of the TGFβ1/TGFβ1R axis (observed following MT1 and MT2 knockout) agree with our previous studies showing that enhanced expression of biliary TGFβ1/TGFβ1R signaling (observed during cholestasis) induces an increase in cholangiocyte senescence and liver fibrosis by enhanced release of TGFβ1. This finding

is important in the progression of a number of cholangiopathies, such as PSC and PBC (10, 13, 25, 36–38). The increase in TGFβ1 signaling (e.g., following MT1/GPR50 heterodimer formation) may contribute to increased cAMP/p-PKA signaling, as suggested by studies in other cell types such as rat intraglomerular mesangial and osteoblast-like cells (39, 40). We next performed studies to demonstrate that the effects of MT1/MT2/TGFβ1 signaling on liver phenotypes are linked to changes in miR-200b-dependent angiogenesis. This signaling pathway plays an essential role in melatonin's impact on biliary/liver phenotypes (3, 10). Supporting this, bioinformatic predictions and luciferase reporter assay found VEGF to be a target of miR-200b (41). Furthermore, miR-200b targets TGFβ1, as well as Smad2 and Snail, which are critical mediators of TGFβ and VEGF signaling (10, 38, 42).

We demonstrated that MT1/MT2 differential modulation of biliary damage and liver fibrosis are associated with changes in the expression of selected clock genes, since downregulation of MT1 reduces the expression of clock genes that are otherwise upregulated by knockout of MT2. We have shown that: (i) the expression of the clock genes, Clock, Bmal1, Cry1, and Per1 is increased in BDL and Mdr2$^{-/-}$ mice; and (ii) melatonin administration or maneuvers (such as pinealectomy or exposure to darkness) that modulate melatonin secretion reduces liver phenotypes by downregulation of miR-200b-dependent angiogenesis (3, 10). Similar to our findings, dysregulation of clock genes is shown in several liver diseases such as NAFLD, NASH, PBC, PSC and alcohol-induced liver damage (8, 43, 44).

In conclusion, while the loss of MT1 decreases liver damage in cholestasis, loss of MT2 alone or together with MT1 worsens biliary senescence and liver fibrosis by the preferential formation of MT1/GPR50 heterodimers, leading to reduced melatonin binding to MT1 and enhanced p-PKA/TGFβ1 axis. Our data suggests that downregulation of MT1/GPR50 signaling may be a critical therapeutic approach for modulating cholangiopathies such as PSC.

Supplementary Material

Refer to Web version on PubMed Central for supplementary material.

Acknowledgments

This work was supported by the Hickam Endowed Chair, Gastroenterology, Medicine, Indiana University, the Indiana University Health - Indiana University School of Medicine Strategic Research Initiative, the VA Merit awards to GA (5I01BX000574) and HF (1I01BX003031) from the United States Department of Veteran's Affairs, Biomedical Laboratory Research and Development Service and NIH grants DK108959 and DK119421 (HF), DK054811, DK115184, DK076898, DK107310, DK110035, DK062975 and AA028711 (GA and SG) and the PSC Partners Seeking a Cure (GA) and by Sapienza University funds #RM1181642BEF570E to PO. This material results from work supported by resources at the Central Texas Veterans Health Care System, Temple, TX, Richard L. Roudebush VA Medical Center, Indianapolis, IN, and Medical Physiology, Medical Research Building, Temple, TX. The views expressed in this article are those of the authors and do not necessarily represent the Department of Veterans Affairs views.

Abbreviations:

PSC	primary sclerosing cholangitis
PBC	primary biliary cholangitis

IBDM	intrahepatic biliary mass
MT1	melatonin receptor 1A
MT2	melatonin receptor 1B
GPR50	G Protein-Coupled Receptor 50
TGFβ	transforming growth factor-β
TGFβR1	TGFβ receptor type I
AANAT	serotonin N-acetyltransferase
Mdr2$^{-/-}$	multidrug resistance 2 knockout
KO	knockout
DKO	MT1/MT2 double knockout
WT	wild-type
BDL	bile duct ligation
HSCs	hepatic stellate cells
LCM	laser capture microscopy
CK-19	cytokeratin-19
SEM	standard error
HNF4α	hepatocyte nuclear factor 4α
H&E	hematoxylin and eosin
α-SMA	α-smooth muscle actin
Col1	collagen type I
Col1a1	collagen type I, alpha 1
p16	cyclin-dependent kinase inhibitor 2A
p21	cyclin-dependent kinase inhibitor 1A
Fn-1	fibronectin-1
SASPs	senescence-associated secretory phenotypes
SA-β-gal	senescence-associated β-galactosidase
CD31	platelet endothelial cell adhesion molecule
Bmal1	brain and muscle ARNT-Like 1
Clock	circadian locomotor output cycles kaput

Cry1	cryptochrome 1
Per1	period circadian clock 1
ALP	alkaline phosphatase
ALT	alanine aminotransferase
PKA	protein kinase A
TCA	taurocholic acid
TβMCA	tauro-β-muricholic acid
GLCA	glycolithocholic acid
DCA	deoxycholic acid
TCDCA	taurochenodeoxycholic acid
TUDCA	tauroursodeoxycholic acid
T-ω-MCA	tauro-ω-muricholic acid
NAFLD	non-alcoholic fatty liver diseases
NASH	nonalcoholic steatohepatitis

REFERENCES

1. Renzi A, DeMorrow S, Onori P, Carpino G, Mancinelli R, Meng F, Venter J, et al. Modulation of the biliary expression of arylalkylamine N-acetyltransferase alters the autocrine proliferative responses of cholangiocytes in rats. Hepatology 2013;57:1130–1141. [PubMed: 23080076]
2. Renzi A, Glaser S, Demorrow S, Mancinelli R, Meng F, Franchitto A, Venter J, et al. Melatonin inhibits cholangiocyte hyperplasia in cholestatic rats by interaction with MT1 but not MT2 melatonin receptors. Am J Physiol Gastrointest Liver Physiol 2011;301:G634–643. [PubMed: 21757639]
3. Chen L, Zhou T, Wu N, O'Brien A, Venter J, Ceci L, Kyritsi K, et al. Pinealectomy or light exposure exacerbates biliary damage and liver fibrosis in cholestatic rats through decreased melatonin synthesis. Biochim Biophys Acta Mol Basis Dis 2019;1865:1525–1539. [PubMed: 30890428]
4. Sugden D, Davidson K, Hough KA, Teh MT. Melatonin, melatonin receptors and melanophores: a moving story. Pigment Cell Res 2004;17:454–460. [PubMed: 15357831]
5. Li DY, Smith DG, Hardeland R, Yang MY, Xu HL, Zhang L, Yin HD, et al. Melatonin receptor genes in vertebrates. Int J Mol Sci 2013;14:11208–11223. [PubMed: 23712359]
6. Levoye A, Dam J, Ayoub MA, Guillaume JL, Couturier C, Delagrange P, Jockers R. The orphan GPR50 receptor specifically inhibits MT1 melatonin receptor function through heterodimerization. EMBO J 2006;25:3012–3023. [PubMed: 16778767]
7. Wojciech S, Ahmad R, Belaid-Choucair Z, Journe AS, Gallet S, Dam J, Daulat A, et al. The orphan GPR50 receptor promotes constitutive TGFbeta receptor signaling and protects against cancer development. Nat Commun 2018;9:1216. [PubMed: 29572483]
8. Baiocchi L, Zhou T, Liangpunsakul S, Ilaria L, Milana M, Meng F, Kennedy L, et al. Possible application of melatonin treatment in human diseases of the biliary tract. Am J Physiol Gastrointest Liver Physiol 2019;317:G651–G660. [PubMed: 31509434]
9. Han Y, DeMorrow S, Invernizzi P, Jing Q, Glaser S, Renzi A, Meng F, et al. Melatonin exerts by an autocrine loop antiproliferative effects in cholangiocarcinoma: its synthesis is reduced

favoring cholangiocarcinoma growth. Am J Physiol Gastrointest Liver Physiol 2011;301:G623–633. [PubMed: 21778461]

10. Wu N, Meng F, Zhou T, Han Y, Kennedy L, Venter J, Francis H, et al. Prolonged darkness reduces liver fibrosis in a mouse model of primary sclerosing cholangitis by miR-200b down-regulation. FASEB J 2017;31:4305–4324. [PubMed: 28634212]
11. Glaser S, Lam IP, Franchitto A, Gaudio E, Onori P, Chow BK, Wise C, et al. Knockout of secretin receptor reduces large cholangiocyte hyperplasia in mice with extrahepatic cholestasis induced by bile duct ligation. Hepatology 2010;52:204–214. [PubMed: 20578263]
12. Anisimov VN, Alimova IN, Baturin DA, Popovich IG, Zabezhinski MA, Manton KG, Semenchenko AV, et al. The effect of melatonin treatment regimen on mammary adenocarcinoma development in HER-2/neu transgenic mice. Int J Cancer 2003;103:300–305. [PubMed: 12471612]
13. Wu N, Meng F, Invernizzi P, Bernuzzi F, Venter J, Standeford H, Onori P, et al. The secretin/secretin receptor axis modulates liver fibrosis through changes in transforming growth factor-beta1 biliary secretion in mice. Hepatology 2016;64:865–879. [PubMed: 27115285]
14. Kyritsi K, Kennedy L, Meadows V, Hargrove L, Demieville J, Pham L, Sybenga A, et al. Mast Cells Induce Ductular Reaction Mimicking Liver Injury in Mice Through Mast Cell-Derived Transforming Growth Factor Beta 1 Signaling. Hepatology 2021;73:2397–2410. [PubMed: 32761972]
15. Wan Y, Meng F, Wu N, Zhou T, Venter J, Francis H, Kennedy L, et al. Substance P increases liver fibrosis by differential changes in senescence of cholangiocytes and hepatic stellate cells. Hepatology 2017;66:528–541. [PubMed: 28256736]
16. Naji L, Carrillo-Vico A, Guerrero JM, Calvo JR. Expression of membrane and nuclear melatonin receptors in mouse peripheral organs. Life Sci 2004;74:2227–2236. [PubMed: 14987948]
17. Han D, Wang Y, Chen J, Zhang J, Yu P, Zhang R, Li S, et al. Activation of melatonin receptor 2 but not melatonin receptor 1 mediates melatonin-conferred cardioprotection against myocardial ischemia/reperfusion injury. J Pineal Res 2019;67:e12571. [PubMed: 30903623]
18. Drazen DL, Nelson RJ. Melatonin receptor subtype MT2 (Mel 1b) and not mt1 (Mel 1a) is associated with melatonin-induced enhancement of cell-mediated and humoral immunity. Neuroendocrinology 2001;74:178–184. [PubMed: 11528219]
19. Gerdin MJ, Masana MI, Rivera-Bermudez MA, Hudson RL, Earnest DJ, Gillette MU, Dubocovich ML. Melatonin desensitizes endogenous MT2 melatonin receptors in the rat suprachiasmatic nucleus: relevance for defining the periods of sensitivity of the mammalian circadian clock to melatonin. FASEB J 2004;18:1646–1656. [PubMed: 15522910]
20. Gerdin MJ, Masana MI, Dubocovich ML. Melatonin-mediated regulation of human MT(1) melatonin receptors expressed in mammalian cells. Biochem Pharmacol 2004;67:2023–2030. [PubMed: 15135299]
21. Aust S, Jager W, Kirschner H, Klimpfinger M, Thalhammer T. Pancreatic stellate/myofibroblast cells express G-protein-coupled melatonin receptor 1. Wien Med Wochenschr 2008;158:575–578. [PubMed: 18998076]
22. Mathes AM, Heymann P, Ruf C, Huhn R, Hinkelbein J, Volk T, Fink T. Endogenous and Exogenous Melatonin Exposure Attenuates Hepatic MT1 Melatonin Receptor Protein Expression in Rat. Antioxidants (Basel) 2019;8.
23. Shajari S, Laliena A, Heegsma J, Tunon MJ, Moshage H, Faber KN. Melatonin suppresses activation of hepatic stellate cells through RORalpha-mediated inhibition of 5-lipoxygenase. J Pineal Res 2015;59:391–401. [PubMed: 26308880]
24. Wu N, Meng F, Zhou T, Venter J, Giang TK, Kyritsi K, Wu C, et al. The Secretin/Secretin Receptor Axis Modulates Ductular Reaction and Liver Fibrosis through Changes in Transforming Growth Factor-beta1-Mediated Biliary Senescence. Am J Pathol 2018;188:2264–2280. [PubMed: 30036520]
25. Zhou T, Wu N, Meng F, Venter J, Giang TK, Francis H, Kyritsi K, et al. Knockout of secretin receptor reduces biliary damage and liver fibrosis in Mdr2(−/−) mice by diminishing senescence of cholangiocytes. Lab Invest 2018;98:1449–1464. [PubMed: 29977037]

26. Ostrycharz E, Wasik U, Kempinska-Podhorodecka A, Banales JM, Milkiewicz P, Milkiewicz M. Melatonin Protects Cholangiocytes from Oxidative Stress-Induced Proapoptotic and Proinflammatory Stimuli via miR-132 and miR-34. Int J Mol Sci 2020; :18;21(24):E9667. doi: 9610.3390/ijms21249667. [PubMed: 33352965]
27. Sanchez-Hidalgo M, de la Lastra CA, Carrascosa-Salmoral MP, Naranjo MC, Gomez-Corvera A, Caballero B, Guerrero JM. Age-related changes in melatonin synthesis in rat extrapineal tissues. Exp Gerontol 2009;44:328–334. [PubMed: 19233254]
28. Hu C, Zhao L, Tao J, Li L. Protective role of melatonin in early-stage and end-stage liver cirrhosis. J Cell Mol Med 2019;23:7151–7162. [PubMed: 31475778]
29. Ou TH, Tung YT, Yang TH, Chien YW. Melatonin Improves Fatty Liver Syndrome by Inhibiting the Lipogenesis Pathway in Hamsters with High-Fat Diet-Induced Hyperlipidemia. Nutrients 2019;11.
30. Baba K, Benleulmi-Chaachoua A, Journe AS, Kamal M, Guillaume JL, Dussaud S, Gbahou F, et al. Heteromeric MT1/MT2 melatonin receptors modulate photoreceptor function. Sci Signal 2013;6:ra89. [PubMed: 24106342]
31. Peschke E, Muhlbauer E, Musshoff U, Csernus VJ, Chankiewitz E, Peschke D. Receptor (MT(1)) mediated influence of melatonin on cAMP concentration and insulin secretion of rat insulinoma cells INS-1. J Pineal Res 2002;33:63–71. [PubMed: 12153439]
32. Wan Y, McDaniel K, Wu N, Ramos-Lorenzo S, Glaser T, Venter J, Francis H, et al. Regulation of Cellular Senescence by miR-34a in Alcoholic Liver Injury. Am J Pathol 2017;187:2788–2798. [PubMed: 29128099]
33. Chen L, He X, Zhang Y, Chen X, Lai X, Shao J, Shi Y, et al. Melatonin receptor type 1 signals to extracellular signal-regulated kinase 1 and 2 via Gi and Gs dually coupled pathways in HEK-293 cells. Biochemistry 2014;53:2827–2839. [PubMed: 24724723]
34. Sampaio Lde F Melatonin inhibitory effect on cAMP accumulation in the chick retina development. Int J Dev Neurosci 2008;26:277–282. [PubMed: 18343081]
35. Ayoub MA, Levoye A, Delagrange P, Jockers R. Preferential formation of MT1/MT2 melatonin receptor heterodimers with distinct ligand interaction properties compared with MT2 homodimers. Mol Pharmacol 2004;66:312–321. [PubMed: 15266022]
36. Tabibian JH, O'Hara SP, Splinter PL, Trussoni CE, LaRusso NF. Cholangiocyte senescence by way of N-ras activation is a characteristic of primary sclerosing cholangitis. Hepatology 2014;59:2263–2275. [PubMed: 24390753]
37. Kennedy L, Francis H, Invernizzi P, Venter J, Wu N, Carbone M, Gershwin ME, et al. Secretin/secretin receptor signaling mediates biliary damage and liver fibrosis in early-stage primary biliary cholangitis. FASEB J 2019;33:10269–10279. [PubMed: 31251081]
38. Kyritsi K, Francis H, Zhou T, Ceci L, Wu N, Yang Z, Meng F, et al. Downregulation of p16 Decreases Biliary Damage and Liver Fibrosis in the Mdr2(−/−) Mouse Model of Primary Sclerosing Cholangitis. Gene Expr 2020;20:89–103. [PubMed: 32393417]
39. Schneider HG, Michelangeli VP, Frampton RJ, Grogan JL, Ikeda K, Martin TJ, Findlay DM. Transforming growth factor-beta modulates receptor binding of calciotropic hormones and G protein-mediated adenylate cyclase responses in osteoblast-like cells. Endocrinology 1992;131:1383–1389. [PubMed: 1324161]
40. Zou R, Xu G, Liu XC, Han M, Jiang JJ, Huang Q, He Y, et al. PPARgamma agonists inhibit TGF-beta-PKA signaling in glomerulosclerosis. Acta Pharmacol Sin 2010;31:43–50. [PubMed: 20037602]
41. McArthur K, Feng B, Wu Y, Chen S, Chakrabarti S. MicroRNA-200b regulates vascular endothelial growth factor-mediated alterations in diabetic retinopathy. Diabetes 2011;60:1314–1323. [PubMed: 21357793]
42. Chen Y, Xiao Y, Ge W, Zhou K, Wen J, Yan W, Wang Y, et al. miR-200b inhibits TGF-beta1-induced epithelial-mesenchymal transition and promotes growth of intestinal epithelial cells. Cell Death Dis 2013;4:e541. [PubMed: 23492772]
43. Saran AR, Dave S, Zarrinpar A. Circadian Rhythms in the Pathogenesis and Treatment of Fatty Liver Disease. Gastroenterology 2020;158:1948–1966 e1941. [PubMed: 32061597]

44. Montagnese S, Nsemi LM, Cazzagon N, Facchini S, Costa L, Bergasa NV, Amodio P, et al. Sleep-Wake profiles in patients with primary biliary cirrhosis. Liver Int 2013;33:203–209. [PubMed: 23173839]

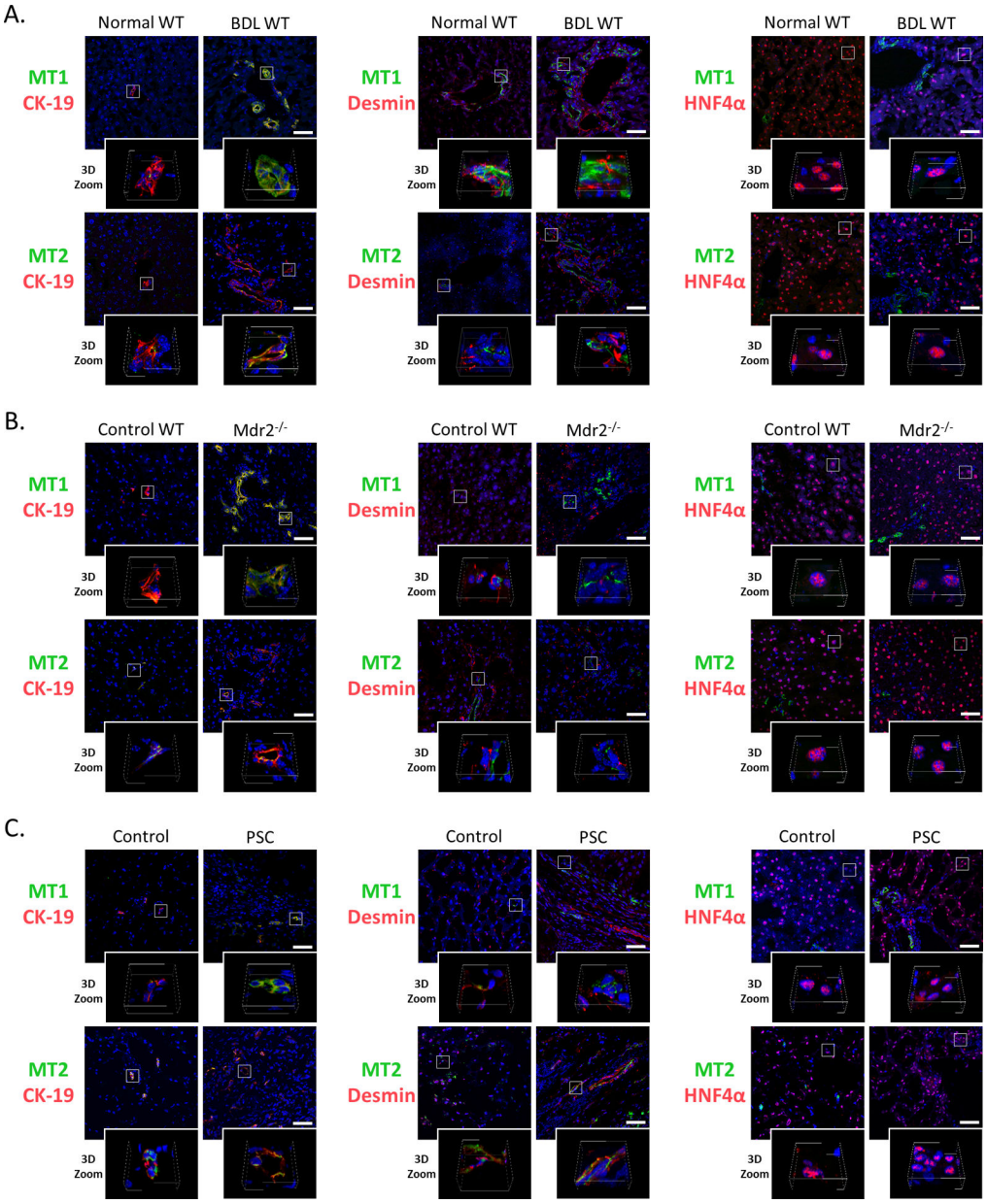

Figure 1.

Immunofluorescence of MT1 and MT2 (co-stained with CK-19, desmin and HNF4α) in liver sections from [**A**] BDL and [**B**] Mdr2$^{-/-}$ mice (and the corresponding control mice) and from [**C**] PSC patients and controls (n=3/group; green: MT1 or MT2, red: CK-19, desmin or HNF4α, blue: DAPI; Orig. Magn., 40x; scale bar = 50 μm; 3D Zoom x10).

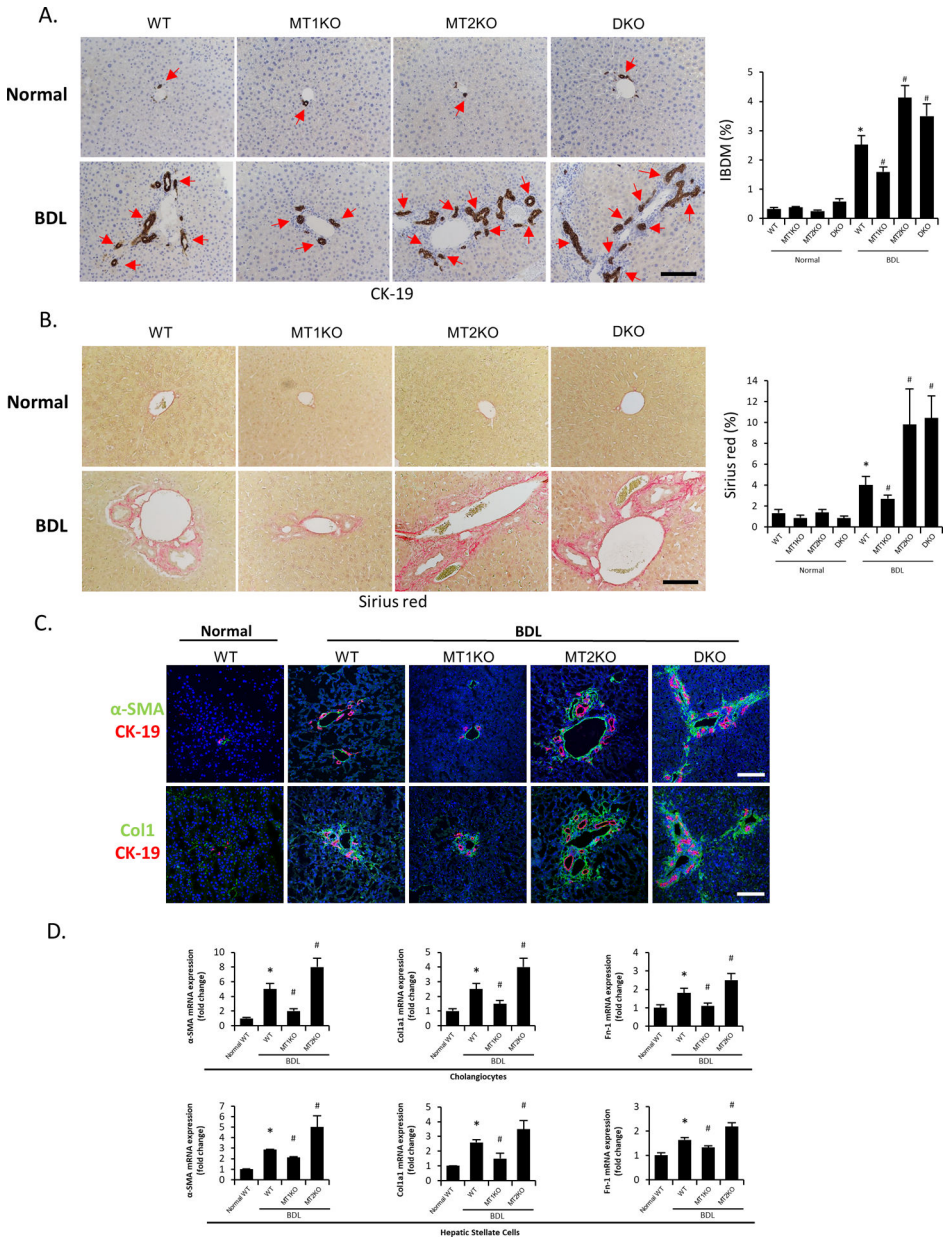

Figure 2.

[**A-B**] Representative images of liver sections from selected mouse groups were examined for [**A**] IBDM by immunohistochemistry of CK-19 and [**B**] collagen deposition by Sirius Red staining (10 different fields from 3 different mice/group; red arrows represent bile ducts; Orig. Magn., 20x; scale bar = 100 μm). [**C**] The immunoreactivity of fibrotic markers α-SMA and Col1 was evaluated by immunofluorescence in mouse liver sections co-stained with CK-19 (n=3/mouse group; green: α-SMA or Col1, red: CK-19, blue: DAPI; Orig. Magn., 20x; scale bar = 100 μm). [**D**] The mRNA expression of fibrotic markers (Col1a1, α-SMA and Fn1) was evaluated by real-time PCR in isolated cholangiocytes (n≥6) and LCM-isolated HSCs (n=3) from the selected mouse groups. For bar graphs, data are mean ± SEM. *P<0.05 vs. WT mice, $^{\#}P$<0.05 vs. BDL WT mice.

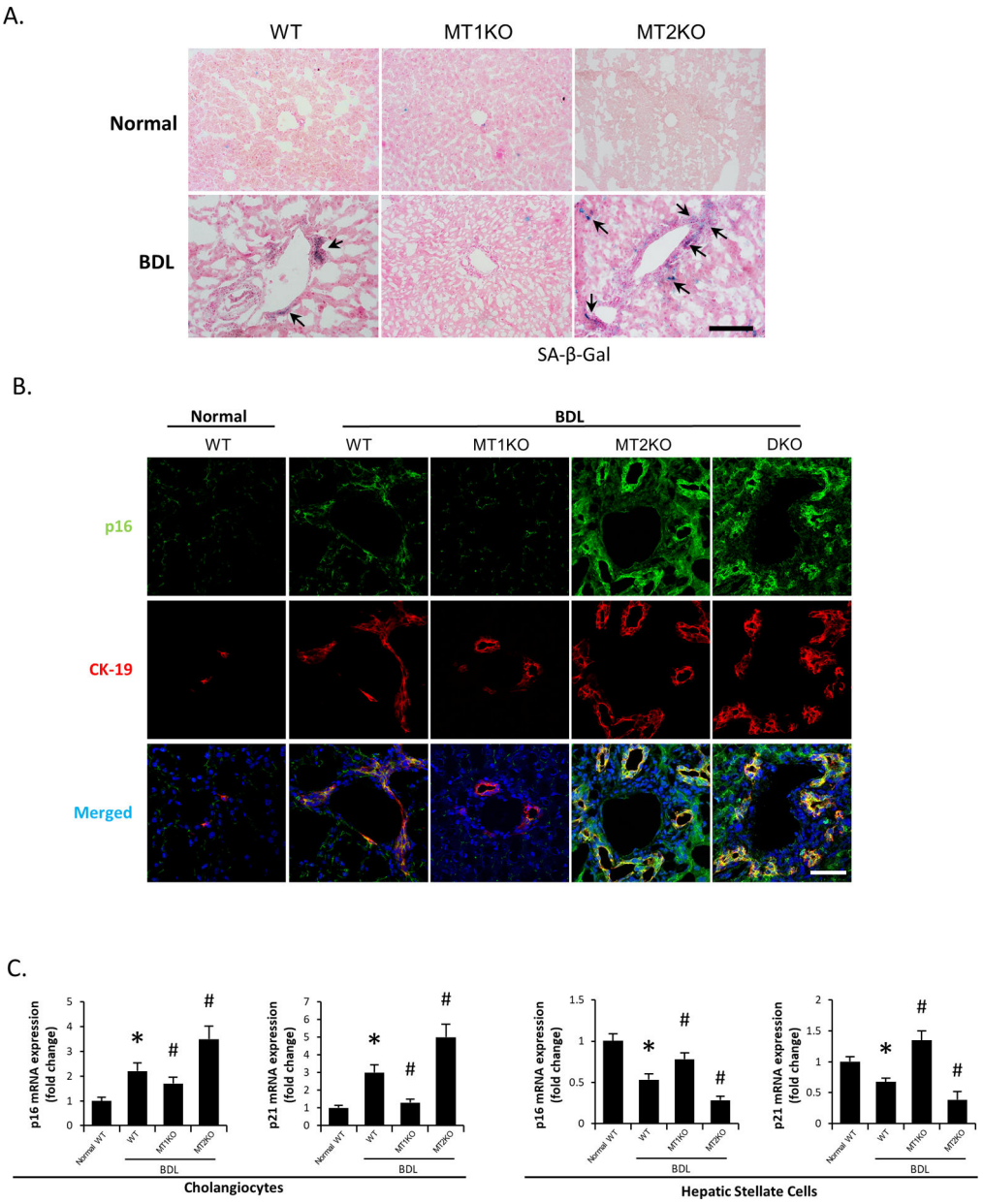

Figure 3.

[**A**] Biliary senescence in liver sections from selected mouse groups was measured by SA-β-gal staining (n=3/mouse group; black arrows represent SA-β-gal-positive bile ducts; Orig. Magn., 20x; scale bar = 100 μm). [**B**] Immunofluorescence for p16 co-stained with CK-19 in selected mouse frozen liver sections (n=3/mouse group; green: p16, red: CK-19, blue: DAPI; Orig. Magn., 60x; scale bar = 50 μm). [**C**] Real-time PCR for senescence markers (p16 and p21) in purified cholangiocytes (n≥6) and LCM-isolated HSCs (n=3) from the selected mice. Data are mean ± SEM. $^{*}P<0.05$ vs. WT mice, $^{\#}P<0.05$ vs. BDL WT mice.

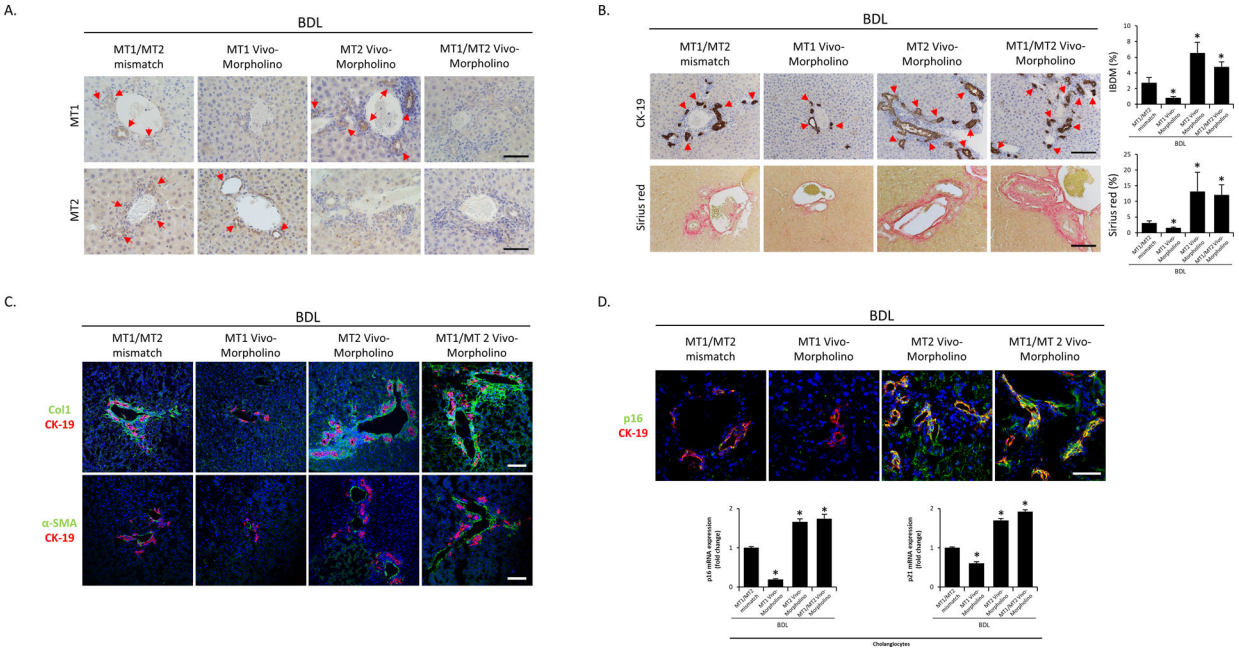

Figure 4.

[**A**] The immunoreactivity and expression of MT1 and MT2 in BDL mice treated with the mismatch Morpholino or MT1, MT2 and MT1/MT2 Morpholino were measured by immunohistochemistry in liver sections (n=3/mouse group; red arrows represent MT1 or MT2-positive bile ducts; Orig. Magn., 40x; scale bar = 50 μm). [**B**] Representative images of liver sections were examined for IBDM by immunohistochemistry of CK-19 and collagen deposition by Sirius Red staining in selected mouse groups (10 different fields from 3 different mice/group; red arrows represent bile ducts; Orig. Magn., 20x; scale bar = 100 μm). [**C**] Liver fibrosis was observed by immunofluorescence of α-SMA and Col1 (co-stained with CK-19) in selected mouse frozen liver sections (n=3/mouse group; green: α-SMA or Col1, red: CK-19, blue: DAPI; Orig. Magn., 20x; scale bar = 100 μm). [**D**] Biliary senescence was observed by immunofluorescence of p16 co-stained with CK-19 in selected mouse frozen liver sections (n=3/mouse group; green: p16, red: CK-19, blue: DAPI; Orig. Magn., 60x; scale bar = 50 μm) and real-time PCR for p16 and p21 in purified cholangiocytes (n≥6). For bar graphs, data are mean ± SEM. **P* <0.05 vs. BDL WT mice treated with MT1/MT2 mismatch Morpholino.

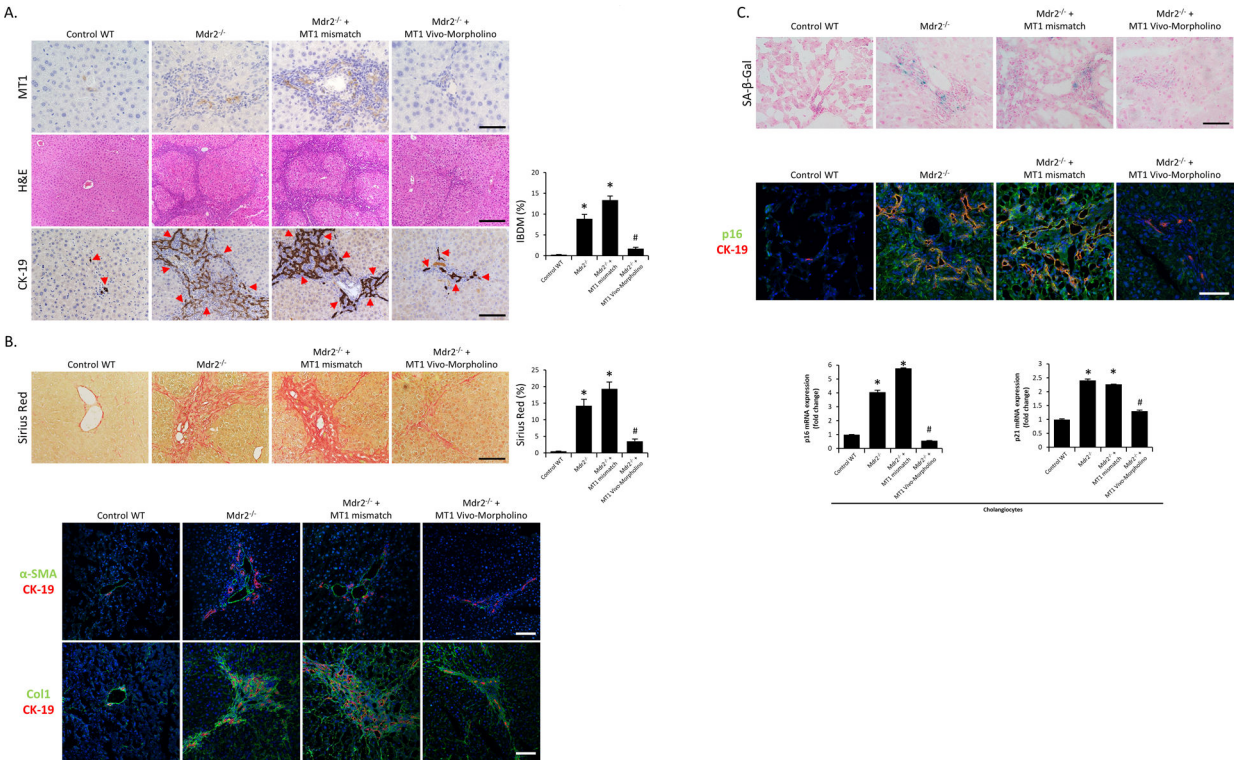

Figure 5.

[**A**] Representative images of liver sections from Mdr2$^{-/-}$ mice (and the corresponding control mice) and mismatch Morpholino or MT1 Vivo-Morpholino treated Mdr2$^{-/-}$ mice were examined for biliary immunoreactivity/expression of MT1 by immunohistochemistry (n=3/mouse group; Orig. Magn., 40x; scale bar = 50 μm), liver damage by H&E staining (n=3/mouse group; Orig. Magn., 10x; scale bar = 200 μm) and IBDM by immunohistochemistry for CK-19 (10 different fields from 3 different mice/group; red arrows represent bile ducts; Orig. Magn., 20x; scale bar = 100 μm). [**B**] Liver fibrosis was observed by Sirius Red staining (10 different fields from 3 different mice/group; Orig. Magn., 20x; scale bar = 100 μm) and immunofluorescence of α-SMA and Col1 (co-stained with CK-19) in selected mouse frozen liver sections (n=3; green: α-SMA or Col1, red: CK-19, blue: DAPI; Orig. Magn., 20x; scale bar = 100 μm). [**C**] Biliary senescence was measured by SA-β-gal staining (n=3/mouse group; Orig. Magn., 40x; scale bar = 50 μm) and immunofluorescence of p16 co-stained with CK-19 in selected mouse frozen liver sections (n=3/mouse group; green: p16, red: CK-19, blue: DAPI; Orig. Magn., 60x; scale bar = 50 μm), as well as real-time PCR for p16 and p21 in purified cholangiocytes (n≥6). For bar graphs, data are mean ± SEM. *P<0.05 vs. WT mice, $^{\#}P$<0.05 vs. Mdr2$^{-/-}$ and Mdr2$^{-/-}$ mice treated with mismatch Morpholino.

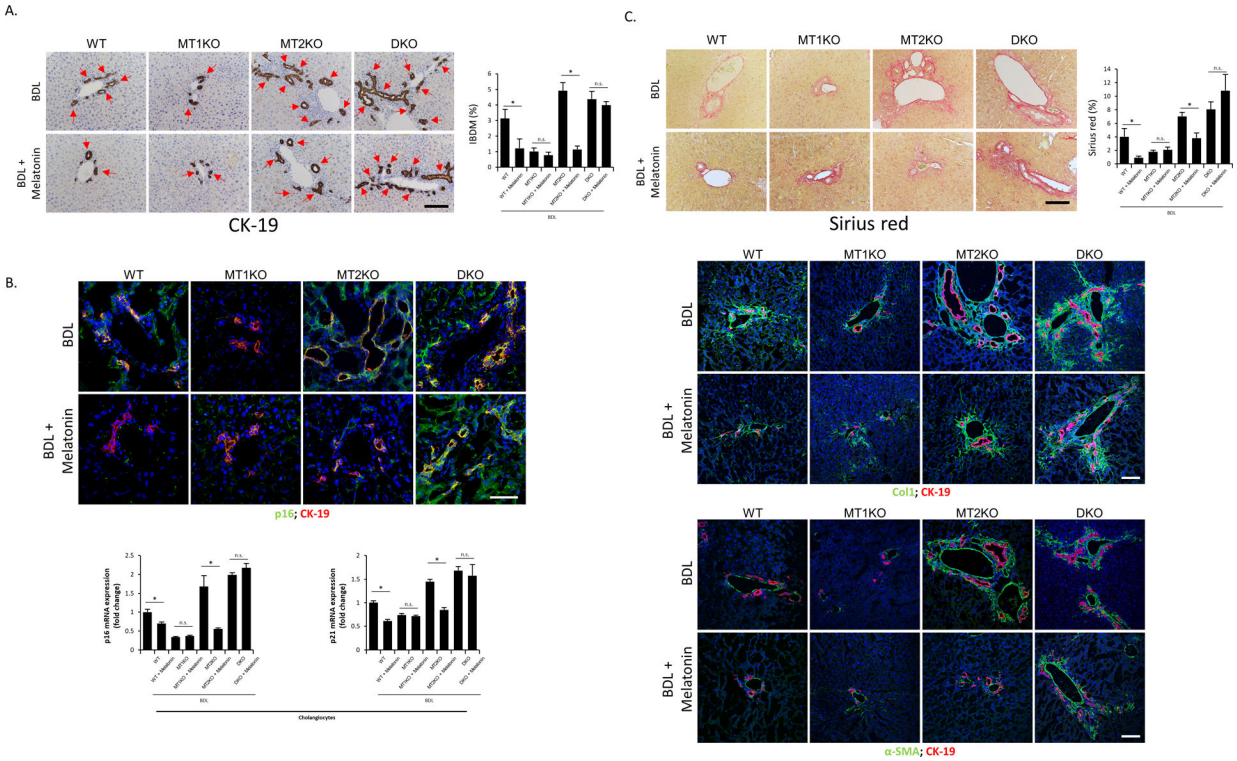

Figure 6.

[**A**] Representative images of liver sections were examined for IBDM by immunohistochemistry of CK-19 from groups of BDL WT, BDL MT1KO, BDL MT2KO and BDL DKO mice treated with/without melatonin (10 different fields from 3 different mice/group; red arrows represent bile ducts; Orig. Magn., 20x; scale bar = 100 μm). [**B**] Biliary senescence was measured by immunofluorescence of p16 co-stained with CK-19 in selected mouse frozen liver sections (n=3/mouse group; green: p16, red: CK-19, blue: DAPI; Orig. Magn., 60x; scale bar = 50 μm) and real-time PCR for p16 and p21 in purified cholangiocytes (n≥6). [**C**] Liver fibrosis was observed by Sirius Red staining (10 different fields from 3 different mice/group; Orig. Magn., 20x; scale bar = 100 μm) and immunofluorescence of α-SMA and Col (co-stained with CK-19) in selected mouse frozen liver sections (n=3; green: α-SMA or Col1, red: CK-19, blue: DAPI; Orig. Magn., 20x; scale bar = 100 μm). For bar graphs, data are mean ± SEM. **P* <0.05 vs. corresponding untreated mice, n.s.= no significant difference.

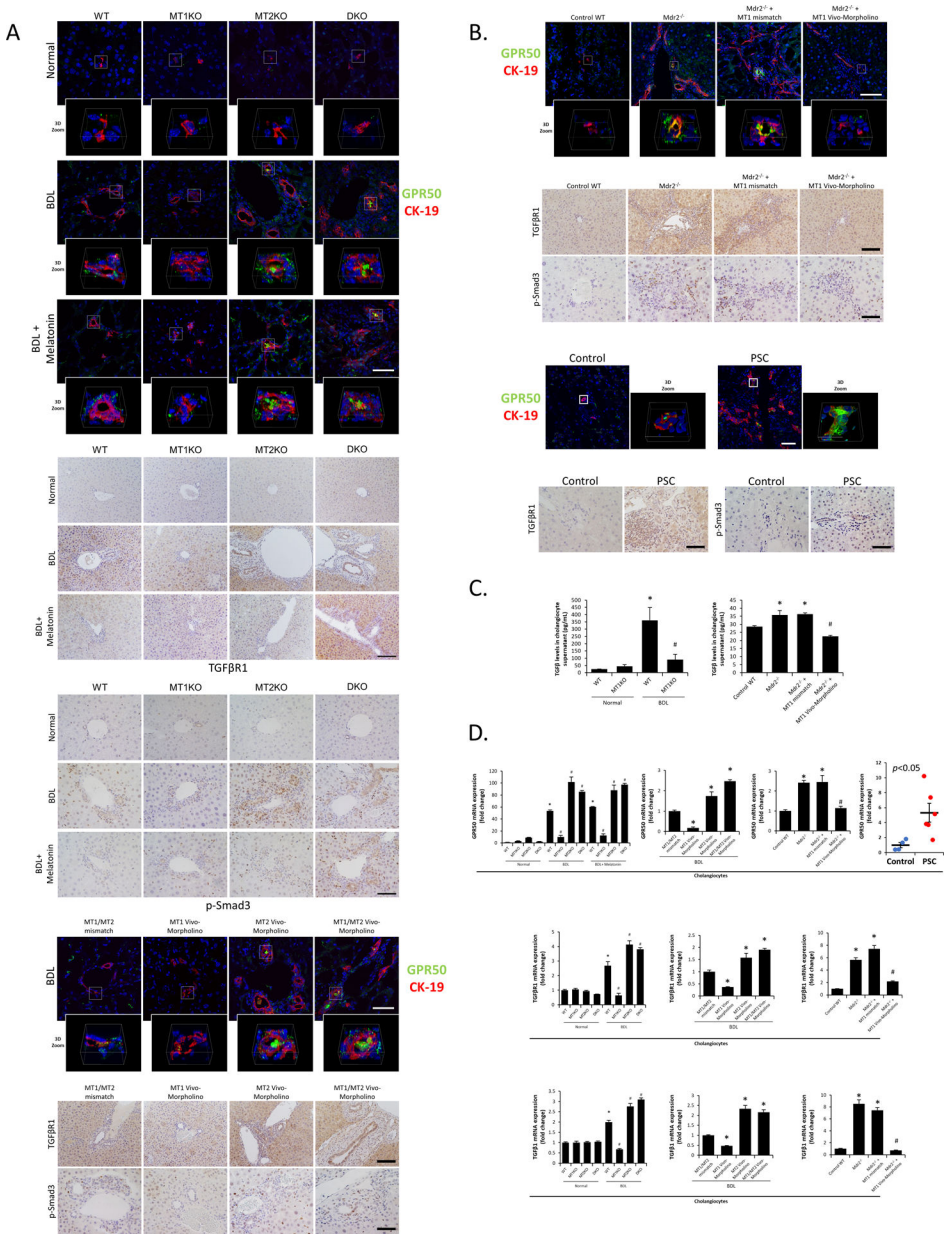

Figure 7.

[**A-B**] Immunoreactivity of GPR50 was measured by immunofluorescence co-stained with CK-19 (green: GPR50, red: CK-19, blue: DAPI; Orig. Magn., 60x for mouse groups and 40x for human groups; scale bar = 50 μm; 3D Zoom x6.7) in frozen liver sections, and immunoreactivity of TGFβR1 (Orig. Magn., 20x; scale bar = 100 μm) and Smad3 phosphorylation (Orig. Magn., 40x; scale bar = 50 μm) was examined by immunohistochemistry in paraffin-embedded liver sections from [**A**] BDL and [**B**] $Mdr2^{-/-}$ related mouse groups (n=3), PSC (n=3) and healthy patients (n=3). [**C**] TGFβ level in mouse cholangiocyte supernatant was measured by ELISA kit (n≥6). [**D**] The mRNA expression of GPR50 in isolated cholangiocytes from human PSC patients (n=6) and controls (n=4) and mRNA expression of GPR50, TGFβR1 and TGFβ1 in isolated mouse cholangiocytes were

evaluated by real-time PCR (n≥6). For bar graphs, data are mean ± SEM. *P <0.05 vs. WT mice or BDL WT mice treated with MT1/MT2 mismatch Morpholino, $^{\#}P$ <0.05 vs. BDL WT mice or Mdr2$^{-/-}$ and Mdr2$^{-/-}$ mice treated with mismatch Morpholino.

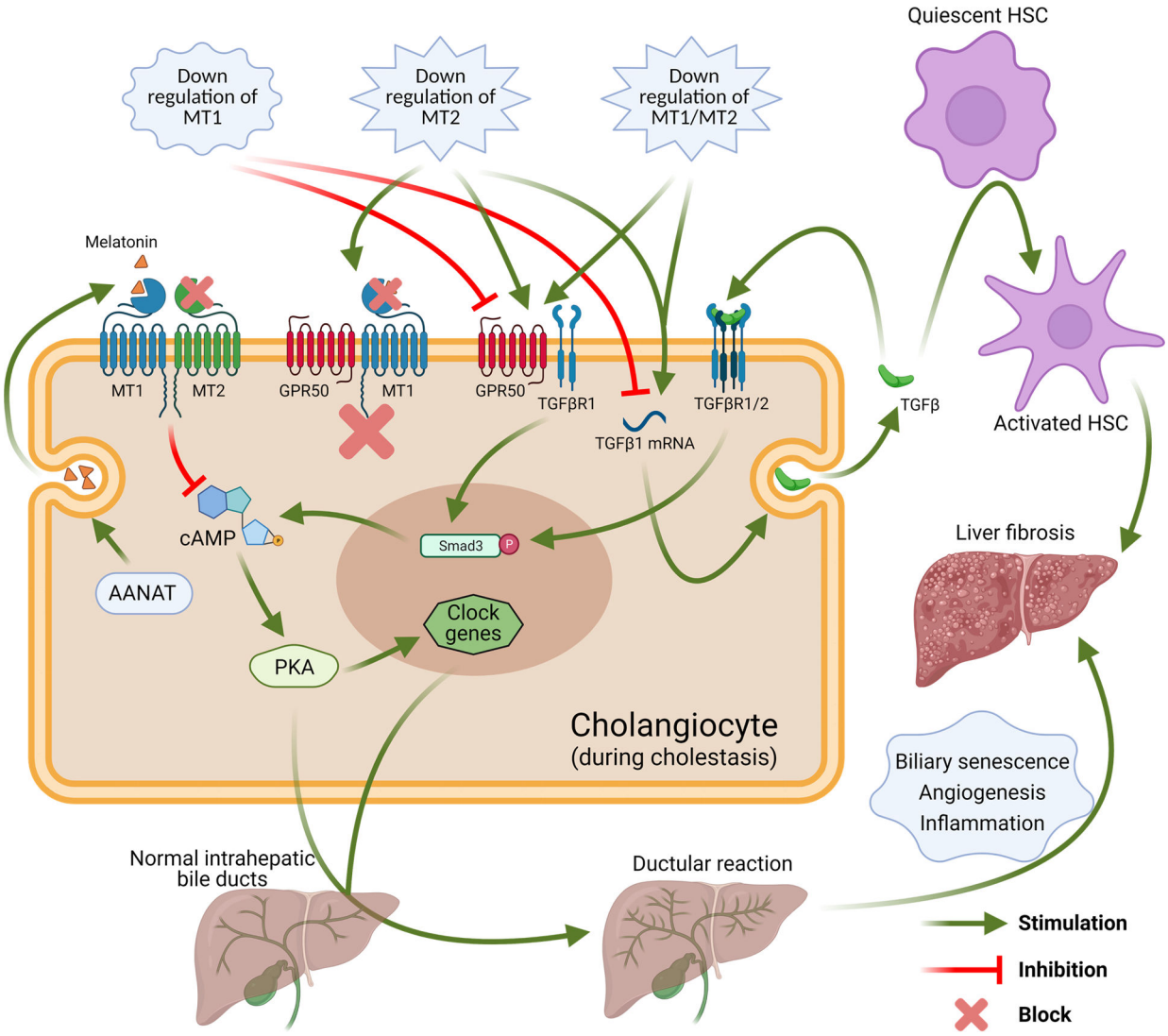

Figure 8.

Working model of down-regulation of MT1 and/or MT2 leads to differential impacts in the biliary expression of clock genes, GPR50, TGFβ, TGFβR1, Smad3 phosphorylation and PKA phosphorylation during cholestasis, which is associated with regulation of ductular reaction, biliary senescence, liver inflammation angiogenesis and fibrosis. (Created with BioRender.com)